MECHANICAL ASSESSMENT OF POROUS MEDIA USING HYBRID SKELETON GRAPH ANALYSIS AND FINITE ELEMENTS. APPLICATION TO TRABECULAR BONE

*G. Aufort *, R. Jennane *, R. Harba *, A. Gasser **, D. Soulat **, C. L. Benhamou ****

* LESI, Laboratoire d'Electronique, Signaux, Images, Université d'Orléans, France
12, rue de Blois, 45067 0rléans CEDEX 2
phone: +33 (0)2 38 41 72 29, fax: +33 (0)2 38 41 72 45, email: gabriel.aufort@univ-orleans.fr
** LMSP, Laboratoire de Mécanique, Systèmes et Procédés, Université d'Orléans, France
*** Equipe INSERM U658, Centre Hospitalier Régional d'Orléans, France

ABSTRACT

The combination of skeletons and Finite Elements (FE) analysis has recently shown its great potential in disordered porous media characterization. A full protocol for creating simplified skeleton-based FE models of large-scale disordered porous media and evaluating their stiffness is presented in this paper. The method uses a sequence of image processing tools. Known algorithms such as curve and surface thinning and shape classification have been improved or adapted to the specific field of porous media analysis. New techniques such as thickness map matching and surface marching cubes triangulation have also been combined. Finally, results from a clinical study on trabecular bone samples emphasize the improvements of the new beam/shell skeleton-based model in comparison to current FE processes.

1. INTRODUCTION

Thinning methodologies have helped during the past 20 years tuning down the scale of large analysis problems, especially porous media characterization. Simplified skeleton-based models have been investigated to retrieve morphological information from large-scale disordered porous media [1] [2]. This work has been shown to be efficient in terms of accuracy, as data is retrieved at a local level [3]. The concept has been pushed forward with the integration of shape information directly into the models [4] [5]. The hybrid skeleton [6] is born from this need to improve the quality of skeleton geometrical properties.

In parallel, this simplification of large porous structures using skeletons inspired researchers to build beam Finite Elements (FE) models [7] [8]. But despite their unquestionable time and computer resource efficiency, they suffered from a significant lack of accuracy. In a very recent work, Lenthe et al. [9] were the first to introduce a geometrical improvement in their beam model by separating rod from plate shapes using a multicolour decomposition technique. However, since they used both the same beam element type for the entire object and an *a priori* model assumption to compute the thickness of the elements, the method can be improved. In fact, since [7] and [8], nobody has been able to correct the geometrical deficiency of simplified FE models. This is the reason why voxel-to-elements FE models are still strongly considered as an unavoidable accuracy reference, despite their huge computing resources requirements [10] [11].

This paper presents a full protocol for evaluating stiffness of large-scale porous media based on the Hybrid Skeleton Graph Analysis technique (HSGA) [12]. Using a shape-dependent skeleton, it decomposes the material into shape primitives, and takes advantage of both beam and shell FE elements to enable a fast and precise mechanical simulation.

This paper is organized as follows: First and foremost, the previous work of HSGA is recalled, including its most recent improvements such as thickness map matching. Then the conversion of the model into FE elements is exposed, using both beam elements for rod shaped structural items and shell elements for plate shaped items. Finally, results from a clinical study of trabecular bone samples are presented, which illustrate the efficiency of the new beam-shell model. Samples from 2 populations are being separated using a statistical hypothesis test to compare the accuracy of the different FE models.

2. PROTOCOL

The work of this paper relies on a previously developed skeleton-based model entitled HSGA, which is presented in a first section. The latest improvement of the technique, the thickness map matching, is explained. The second section describes the protocol used to convert data from the HSGA to FE models, using either beam chains for rod-shaped parts or shell triangulations for plate-shaped parts.

2.1 Hybrid Skeleton Graph Analysis

Despite the intense work that has been carried out on the different ways of skeletonizing objects [13], skeletons are often application-dependent, and consider only one type of object shape. In [2] and [9], the trail of new geometrical thinning criterions has been followed and led to interesting shape-dependent skeletons. The HSGA technique came from this need to consider the complex shape of disordered porous media. Inspired from the Line Skeleton Graph Analysis method (LSGA) [1], HSGA defines a full protocol for modeling porous media composed of rods and plates. As shown on figure 1, it relies on the hybrid skeleton [6], a new adapted thinning procedure that switches between curve thinning and surface thinning patterns, depending on the local shape of the structure [4]. Solving the lack of geometrical accuracy of skeleton-based model's issue, the HSGA has been shown to better reflect micro-architectural changes in trabecular bone samples [12] than the LSGA.

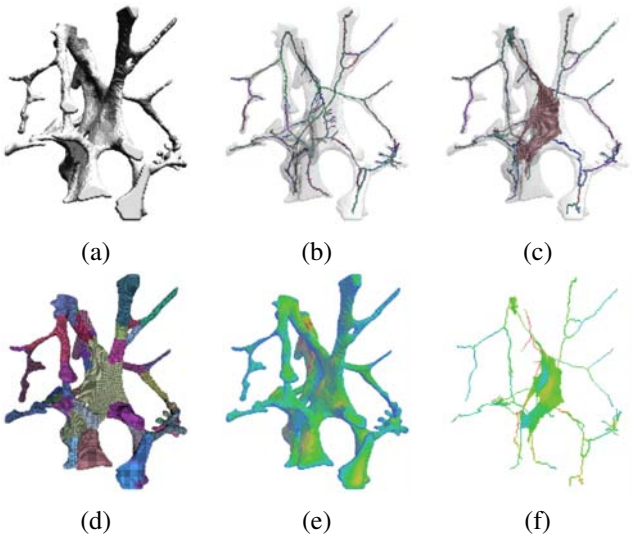

Figure 1: Illustration of HSGA hybrid-skeleton based modeling of disordered porous media: original object (a), an LSGA line-skeleton based model (b), an HSGA hybrid-skeleton based model (c), a region-growth segmented HSGA model (d), the thickness map of the original object (e) and the thickness map matched HSGA model (f)

However, HSGA implements a region growth segmentation process which imposes to use model-dependant characteristics. Indeed, length (L), volume (V), section (S) and thickness (Th) of each item is approximated by guessing the item's accordance to a cylinder or a parallelepiped. Recently, we introduced an improvement to the HSGA segmentation method by replacing the region-growth as used in [5] and [12] by a new method called "thickness map matching". It consists in integrating local cross-section information coming from the object's thickness map [14] directly into the HSGA model using a simple voxel-to-voxel matching process (see figure 1). The thickness map technique, based on distance transforms, has the advantage of not using any *a priori* model assumption to compute item properties, especially cross-section for rods and thickness for plates.

In this paper, we used the HSGA as a basis for the generation of FE models. Thickness map matching was processed to improve the geometrical accuracy of all generated FE models using local cross-section values.

2.2 Finite Elements conversion

The reference for Finite Elements (FE) analysis of discrete samples is unquestionably the voxel-to-element conversion as evoked in many papers [10] [11]. But in the case of skeleton-based models, other type of elements can be used to simplify large-scale problems and gain computing time and resources. In this paragraph, we explain our modeling choices, relative to the compromise between simplification and loss of accuracy in the simulation. First, the method used to convert rod shapes to beam chains is explained. Then the triangulation technique used to convert plate shapes to shell elements is described.

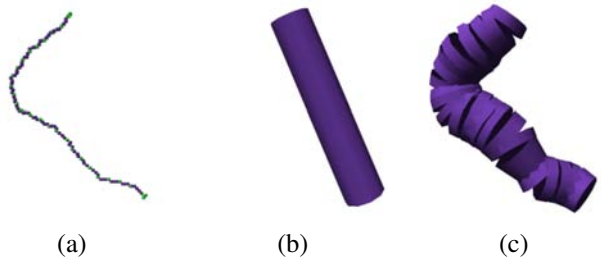

Figure 2: Illustration of the rods to beam elements chains conversion: voxels of the 1D path extracted from its curve skeleton with intermediate nodes (a), simple cylinder model assumption using the rod's volume and skeleton length to compute its section as S = V / l (b), and beam chain modeling of the item using local thicknesses (c)

2.2.1 *Rods to beam elements chains conversion*

The FE that matches the geometry of a straight rod is the beam element. Its geometry is described as a 1D segment, which is assigned a circular cross section. This technique has first been investigated by [8] to assess the stiffness of trabecular bone. However, results have shown that modeling bone by a simple rod network is not sufficient to get a precise stiffness evaluation, due to geometrical lack of accuracy. Lenthe et al. [9] have explored this field of beam-modeling rod shapes in porous media, but did not resolve the shape accuracy issues.

In order to convert a rod item to FE, we introduced the "beam chains"concept [15]. Inspired from a feature extraction technique used in the field of 3D animation [16], the beam chain introduces evenly set intermediate nodes on the curve skeleton as can be seen in figure 2. This process is called "splitting"as it breaks the curve into small segments that better match the curvature of the rod item. Finally, each splitted element (i.e. each effective beam FE) is assigned a section according to the local thickness values, as illustrated in figure 2.

2.2.2 *Plates to shell elements conversion*

Plate zones are badly described in the case of beam-only models [8] [15], which lead to a non-negligible bias for morphological results [12]. It is suspected that this lack of geometrical accuracy also alters mechanical results. In fact, modeling plates is much more challenging than modeling rods, since no work has really been done on this field. Recently, Lenthe et al. [9] had the idea of converting a plate into a set of beams instead of a single beam. Yet, the efficiency of this conversion can be discussed, since the notion of beam set is not geometrically obvious, and the beam sections are model-dependent. We present here an original approach that gather the power of a new triangulation method and a better choice of FE type to improve plate modeling.

The FE used to describe planar shapes is the shell element. It is defined as a 2D medial surface geometry (either triangle or quad strips for example), on which each element is assigned a thickness value. The stake in this case was to be able to transform the 26-connected plate voxels sets into a list of simple 2D primitives like triangles or quads. Meshing isosurfaces has been widely explored in computer graphics since the early 80's, leading to a great range of techniques:

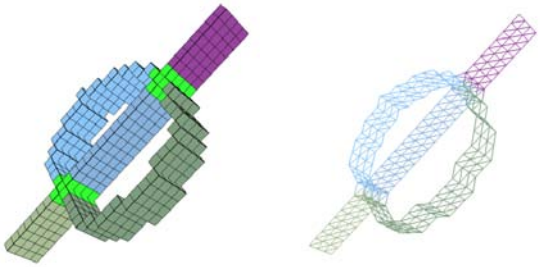

(a) (b)

Figure 3: Illustration of the plates to shell elements conversion: 26-connex voxels of the 2D surface extracted from its surface skeleton (a), and example of a shell elements triangulation using Surface Marching Cubes (b)

surface fitting, surface tracking (also known as continuation methods) and spatial sampling. However, the case of crossing and stacking manifold surfaces from disordered data is still difficult to handle with criterions like Delaunay tracking, and none of these techniques suited our needs. We chose to inspire from a famous spatial sampling method: Marching Cubes (MC) [17], which subdivises space into cells and search those that intersect the implicit surface. Our algorithm, called Surface Marching Cubes (SMC), compute the full-resolution triangulation of any 26-connected surface by following the MC principle while using a new set of neighbourhood patterns. All the triangles linking the voxels of the surface are generated. Figure 3 presents the result of the triangulation of a simple 26-connex surface set. Finally, each shell element (i.e. each triangle) is assigned a section according to the local thickness value in the thickness map, just as we did for the beam elements in the case of rod shapes.

3. CLINICAL STUDY

The HSGA-based Finite Elements conversion method has been applied to the field of trabecular bone characterization. In order to compare the efficiency of the different skeleton-based FE models including HSGA, we relied on medical bone data with an *a priori* knowledge of fracture risk. The medical staff at the hospital of Orleans provided us 2 populations of each 9 samples extracted from post-mortem femoral head and acquired using a SkyScan micro-scanner. The first 9 OP samples have been extracted from osteoporotic patients with known bone fracture risk. The other 9 came from coxarthric patients, which bone structure is known to be hypertrophied. The characteristics of the 2 populations are previously known, so they can be used to verify the separating power of any feature that is said to reflect the bone microarchitecture alterations. Figure 4 shows 2 extracts from an OA and an OP sample.

After slides reconstruction, the discrete samples were pre-processed to 200^3 isotropic voxel sized cubes, with a resolution of 24.04 μm per voxel side (i.e. 4.568 mm^3 for each sample). Pre-processing ensured that each sample was perfectly biphasic (solid phase representing bone vs. pore phase in the background), and contained only 1 connex solid phase. 26/6 connexity was assumed (as 26- for solid phase and 6-connexity for background). Further information about these operations can be found in [6] [12] and [18].

First, LSGA and HSGA analysis has been processed on

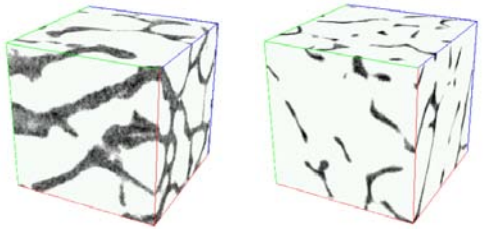

OA OP

Figure 4: 64^3 voxels extracts of samples from the 2 populations to illustrate the microarchitectural differences in coxarthric (OA) and osteoporotic (OP) trabecular bones

each of the 18 samples. Mean features have been extracted from each model: Rod volume (Ro.V), Rod length (Ro.L), Rod thickness (Ro.Th), Plate volume (Pl.V), Plate surface (Pl.S), Plate thickness (Pl.Th). Results from well established clinical methods like Mean Intercept Length (MIL) [19] are also computed in comparison purposes: Bone Mineral Density (BMD, defined as Bone Volume over Total Volume, BV/TV), Bone Surface over Total Volume (BS/TV), Bone Surface over Bone Volume (BS/BV), MIL's Trabecular Number (Tb.N), MIL's Trabecular Spacing (Tb.Sp), MIL's Trabecular Thickness (Tb.Th), Connectivity Density (Conn.D). Mean and standard deviation values of each feature for the 2 populations are presented in table 1.

A bilateral hypothesis test [20] was used to evaluate each feature's discrimination power. Considering a freedom degree of 16 and a significance level of $\alpha = 0.01$, any parameter is said to separate the 2 populations if the Student's $|t|$ value exceeds 2.92. $|t|$ values corresponding to each feature are also reported in table 1.

Then FE models have been built for each sample from both LSGA and HSGA models: a beam-only model using Pothuaud approach [8], then a beam/shell model using the new technique presented in this paper. For both simplified models (beam and beam/shell), we turned the split properties for rod modeling on and off. Beam and shell elements were converted according to the protocol explained previously in this paper. The aim of generating the serie of 4 models was to investigate the effect of the successive geometrical improvements on the mechanical results as follows:

- LSGA is definitely the simplest way of representing the medium's structure with rods only.
- Splitted LSGA model uses curve splitting to match the rod shape.
- Then HSGA introduces plates in the model.
- Finally, splitted HSGA takes advantage of both beam chains and shell triangulation.

All FE models have been imported into the commercial software *Abaqus* which was used to estimate their apparent Young's Modulus. As the simulation required material definition, we assigned the entire model the same behavior, with a bone tissue characterized by an arbitrary Young's modulus of 15 GPa and a Poisson's coefficient of 0.3. These values are close to those found in the litterature [9] [21]. In this kind of comparative study, the material's behavior does not really matter since measured reaction forces are compared relatively. Once defined, each model was tested in compression in the 3 space directions (x, y and z). Boundary

conditions on the cube's faces were set to zero for translations perpendicular to the faces and their complementary rotations. Complementary translations were also blocked for the 2 faces perpendicular to the compression axis. Then, a displacement value Δl was applied on the compression direction's front face. Small displacement of 2% of the cube's size (i.e. 0.0913 mm) avoided non-linearity issues. The apparent Young's modulus (E_{app}) of the model was then computed [9] as:

$$E_{app} = \frac{\sum RF / l^2}{\Delta l / l}$$

where $\sum RF$ represents the measured sum of the Reaction Forces (RF) on each node of the compression face, l is the size of the cube's side. Estimated apparent Young's modulus values expressed in $N.mm^{-2}$ for each model and each population are reported in table 1.

		feature	OA $mean \pm std$	OP $mean \pm std$	t
Volume	MIL	BMD	0.252 ± 0.050	0.167 ± 0.056	**3.196**
		BS/TV mm^{-1}	3.120 ± 0.339	2.639 ± 0.579	2.029
		BS/BV mm^{-1}	14.066 ± 1.555	18.254 ± 3.251	**3.287**
		Conn.D mm^{-3}	-7.110 ± 2.236	-6.814 ± 3.702	0.194
		Tb.N mm^{-1}	1.820 ± 0.198	1.539 ± 0.338	2.029
		Tb.Sp mm	0.395 ± 0.076	0.566 ± 0.229	2.000
		Tb.Th mm	0.160 ± 0.022	0.124 ± 0.025	**3.068**
Morpho	LSGA	Mean Ro.V mm^3	0.017 ± 0.003	0.012 ± 0.004	2.897
		Mean Ro.L mm	0.379 ± 0.046	0.364 ± 0.066	0.338
		Mean Ro.Th mm	0.252 ± 0.033	0.194 ± 0.027	**3.840**
		Total Ro.V mm^3	9.679 ± 2.962	7.903 ± 1.889	1.430
		Total Pl.V mm^3	18.293 ± 4.765	10.692 ± 4.878	**3.153**
	HSGA	Mean Ro.V mm^3	0.004 ± 0.001	0.005 ± 0.002	1.000
		Mean Ro.L mm	0.220 ± 0.032	0.271 ± 0.080	1.657
		Mean Ro.Th mm	0.249 ± 0.038	0.187 ± 0.025	**3.846**
		Mean Pl.V mm^3	0.048 ± 0.023	$0,050 \pm 0,016$	0.151
		Mean Pl.S mm^2	0.228 ± 0.157	$0,257 \pm 0,108$	0.423
		Mean Pl.Th mm	0.304 ± 0.038	$0,228 \pm 0,040$	**3.895**
LSGA	Non splitted	Nodes number	1249 ± 315	1137 ± 443	0.582
		$E_{app}(x)\ N.mm^{-2}$	166.98 ± 94.38	68.72 ± 47.15	2.636
		$E_{app}(y) N.mm^{-2}$	186.12 ± 98.74	77.86 ± 56.39	2.693
		$E_{app}(z) N.mm^{-2}$	169.99 ± 92.70	91.02 ± 69.77	1.925
	Splitted	Nodes number	3876 ± 679	3343 ± 788	1.452
		$E_{app}(x) N.mm^{-2}$	141.25 ± 82.20	50.13 ± 35.09	2.883
		$E_{app}(y) N.mm^{-2}$	158.15 ± 78.00	57.51 ± 43.18	**3.193**
		$E_{app}(z) N.mm^{-2}$	131.78 ± 71.15	67.99 ± 54.64	2.014
HSGA	Non splitted	Nodes number	138312 ± 31692	94890 ± 37769	2.491
		$E_{app}(x) N.mm^{-2}$	113.96 ± 65.57	$34.06 \pm 16,85$	**3.338**
		$E_{app}(y) N.mm^{-2}$	171.92 ± 102.03	$48.39 \pm 25,55$	**3.322**
		$E_{app}(z) N.mm^{-2}$	111.29 ± 42.98	$58.05 \pm 35,22$	2.708
	Splitted	Nodes number	139058 ± 31556	95753 ± 37580	2.496
		$E_{app}(x) N.mm^{-2}$	112.02 ± 62.85	33.32 ± 17.52	**3.412**
		$E_{app}(y) N.mm^{-2}$	164.02 ± 103.02	34.22 ± 15.84	**3.522**
		$E_{app}(z) N.mm^{-2}$	101.00 ± 41.73	51.13 ± 30.25	2.737

Table 1: Results of the clinical study on trabecular bone samples from 2 pathologically different populations (OA as coxarthric and OP as osteoporotic). Mean and standard deviation values are reported for each extracted feature and for each population. $|t|$ Student's values dicriminating the 2 populations are indicated in the last column. A value of $|t| > 2.92$ is said to be significantly distinctive between osteoporotic and coxarthric patients. The different models (LSGA and HSGA, with and without splitting process) are presented in rows for comparison purposes

4. DISCUSSION

Results from the clinical study are discussed in 2 sections: first morphological comparisons then mechanical issues. Finally, conclusions are drawn and further work is indicated.

In a morphological point of view, Bone Mineral Density measurement is the reference, since it is used in the clinical tomodensitometry routine. In our study, with a value of $|t|_{BMD} = 3.196$, this feature significantly discriminates the 2 populations. However, physicians have demonstrated that bone density covers about 75% of bone biomechanical properties, which leaves 25% of the diagnosis to other parameters such as microarchitectural properties. BS/BV and Tb.Th from the MIL, with respectively $|t|_{BS/BV} = 3.287$ and $|t|_{Tb.Th} = 3.068$, illustrate the fact that there is still useful information to extract from the samples in addition to BMD. In this purpose of microarchitectural characterisation, and on the contrary to MIL global-scale features, skeleton-based techniques such as LSGA and HSGA do not make any model assumption, and measure structural properties at a local level. This is the reason why values of Ro.Th ($|t|_{Ro.Th} = 3.840$ for LSGA and $|t|_{Ro.Th} = 3.846$ for HSGA) and Pl.Th ($|t|_{Pl.Th} = 3.895$, HSGA only) are more precise than MIL, as they better discriminate OA samples from OP samples. Furthermore, these results show the improvements of the HSGA which consider plates in addition to rods. In fact, the LSGA's Ro.Th information is not truthful since it integrates plate information, making an arbitrary shape approximation. Although Ro.Th values are about the same for LSGA and HSGA, Pl.Th is clearly a new discriminative value, which shows the complementarity of such measurements. To conclude about morphological results, including plate information is a real benefit for the HSGA model, which can be shown either by studying local features like Ro.Th and Pl.Th, or a few global features like the Total Plates Volume ($|t|_{Pl.V} = 3.153$).

The apparent Young's modulus (E_{app}) of the 4 FE models have been computed for the 2 populations, for each sample, and for each of the 3 space directions (x, y, and z). At first, we notice that E_{app} values reveal a different material behavior in the 3 compression directions. Thus, there is no possible comparison between directions within a sample. However, it is possible to study the influence of the model's geometry on the apparent Young's modulus between the 2 populations for a given direction (either x, y or z). In this case, the 3 compression directions give us 3 different sets of measures for each FE model.

Since the $|t|$ values rely on the *a priori* knowledge of OP samples fragility in comparison to OA samples, it is assumed that there is a difference in their E_{app} behavior. Figure 5 presents the $|t|_{E_{app}}$ values vs the geometrical precision for the 3 directions, and illustrates the use of this assumption to compare the 4 FE models depending on there geometrical accuracy. First, the $|t|_{E_{app}}$ is increasing with geometrical accuracy which confirms that geometrical improvements in the HSGA also have a significant influence in terms of mechanical accuracy of the models. Then, it can be noticed on table 1 that the $|t|_{E_{app}}$ trend is the same for each of the 3 directions, even if E_{app} values are different. Last but not least, 2 of the 3 directions are able to separate the 2 populations according to the level of significance of $\alpha = 0.01$, increasing $|t|_{E_{app}}$ up to 3.412 and 3.522 with the best model (splitted HSGA).

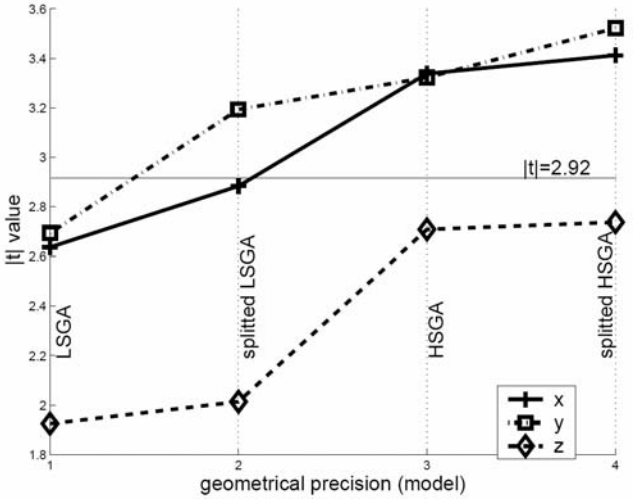

Figure 5: Evolution of the discriminative power $|t|_{E_{app}}$ of the apparent Young's modulus in fonction of the geometrical accuracy of the FE model. In x coordinates the models from simple LSGA to splitted HSGA, ordered by geometrical accuracy. In ordinate the $|t|_{E_{app}}$ value. Each plot represents one of the 3 compression directions along the 3 orthogonal axes

Since the reference voxel-to-elements conversion technique requires huge computing ressources (several millions of elements), our study shows that using a few thousand nodes, skeleton-based models are still able to emphasize apparent Young's modulus differences in trabecular bone. Moreover, we presented a new HSGA shape-dependant FE model using beam and shell elements combination that gives better separation results than beam-only models. Further work is to be carried out on the validation of the simulation of HSGA Finite Elements models. We intend to correlate the simulations using skeleton-based FE models and voxel-to-elements models with the measurement of the real experimental Young's modulus. Plus, the HSGA itself can still be improved, by adding new type of shapes into the hybrid skeleton for example, or by assigning more precise tissue properties to the elements of the FE (using micro-scanner's grey levels for example).

REFERENCES

[1] L. Pothuaud, P. Orion, E. Lespessailles, C. L. Benhamou, and P. Levitz. A new method for three-dimensional skeleton graph analysis of porous media: application to trabecular bone microarchitecture. *J. of Microscopy*, 199(2):149–161, 2000.

[2] P. K. Saha, B. B. Chaudhuri, and D. D. Majumder. A new shape preserving parallel thinning algorithm for 3 d digital images. *Pattern Recognition*, 30:1939Ű–1955, 1997.

[3] L. Pothuaud, A. Laib, P. Levitz, C. L. Benhamou, and S. Majumdar. Three-dimensional-line skeleton graph analysis of high-resolution magnetic resonance images: a validation study from 34-microm-resolution microcomputed tomography. *J Bone Miner Res.*, 17(10):1883–1895, Oct. 2002.

[4] A. Bonnassie, F. Peyrin, and D. Attali. A new method for analyzing local shape in three-dimensional images based on medial axis transformation. *IEEE. Trans. Sys. Man. Cyber.*, 44(4):700–705, 2003.

[5] M. Stauber and R. Muller. Volumetric spatial decomposition of trabecular bone into rods and plates–a new method for local bone morphometry. *Bone*, 38(4):475–484, 2005.

[6] G. Aufort, R. Jennane, R. Harba, and C. L. Benhamou. A new shape-dependant skeletonization method. application to porous media. In *Proc. EUSIPCO 2006*, Florence, Italy, September 2006.

[7] M. Stauber, M. Huber, G. H. Van Lenthe, S. K. Boyd, and R. Muller. A finite element beam-model for efficient simulation of large-scale porous structures. *Comput. Methods Biomech. Biomed. Engin.*, 7(1):9–16, Feb. 2004.

[8] L. Pothuaud, B. V. Rietbergen, C. Charlot, E. Ozhinsky, and S. Majumdar. A new computational efficient approach for trabecular bone analysis using beam models generated with skeletonized graph technique. *Comp. Meth. in Biomech. and Biomed. Eng.*, 7(4):205+, 2004.

[9] H. G. van Lenthe, M. Stauber, and R. Müller. Specimen-specific beam models for fast and accurate prediction of human trabecular bone mechanical properties. *Bone*, 39(6):1182–1189, 2006.

[10] D. Ulrich, B. V. Rietbergen, H. Weinans, and P. Ruegsegger. Finite element analysis of trabecular bone structure: a comparison of image-based meshing techniques. *J. biomech.*, 31(12):1187–1192, 1998.

[11] H. H. Bayraktar. Nonlinear micro finite element analysis of human trabecular bone. *Circle 141 - Abaqus Inc.*, pages 22–25, 2004.

[12] G. Aufort, R. Jennane, and R. Harba. Hybrid skeleton graph analysis of disordered porous media. application to trabecular bone. In *Proc. IEEE ICASSP 2007*, pages II 781–784, Toulouse, France, May 2006.

[13] L. Lam, S.-W. Lee, and C.Y. Suen. Thinning methodologies-a comprehensive survey. *Document image analysis*, pages 61–77, 1995.

[14] T. Hilderbrand and P. Ruegsegger. A new method for the model independent assessment of thickness in three-dimensional images. *J. of Microscopy*, 185:65–67, 1997.

[15] G. Aufort, R. Jennane, R. Harba, A. Gasser, D. Soulat, and C. L. Benhamou. Nouvelle approche de modélisation de milieux poreux. application à lŠos trabéculaire. In *GRETSI'05*, pages 429–432, Louvain-la-Neuve, Belgium, September 2005.

[16] F. Reinders, M. E. D. Jacobson, and F. H. Post. Skeleton graph generation for feature shape description. In *Proc. Data Visualization*, pages 73–82, 2000.

[17] Lorensen W. E. and Cline H. E. Marching cubes: a high resolution 3d surface construction algorithm. *Computer Graphics*, 21:163–169, 1987.

[18] J. Hoshen and R. Kopelman. Percolation and cluster distribution. i. cluster multiple labeling technique and critical concentration algorithm. *Phys. Rev. B*, 14:3438–3445, October 1976.

[19] W. J. Whitehouse. The quantitative morphology of anisotropic trabecular bone. *J. of Microscopy*, 101(2):153–168, 1974.

[20] M. R. Spiegel. *Theory and problems of probability and statistics*. Schaum, McGraw-Hill, New York, 1975.

[21] Bourne B. C. and Van Der Meulen M. C. Finite element models predict cancellous apparent modulus when tissue modulus is scaled from specimen ct-attenuation. *J Biomech.*, 37(5):613–621, May 2004.